1990/021

Institute of Hydrology

Overseas Development Report

[redacted]

Natural Environment Research Council

Infrared thermometry over a sparse millet crop

ICRISAT Sahelian Centre 1987

I. R. Wright

Institute of Hydrology
Maclean Building
Crowmarsh Gifford
Wallingford
Oxon
OX10 8BB

Report No. ODA 90/5
April 1990

Summary

This report describes a pilot study into aspects of infrared thermometry over a sparse millet crop and addresses not only the problems associated with a complex field crop structure, but also the performance of sensitive instrumentation in a harsh tropical climate.

Two types of infrared thermometer and an array of soil thermistors were used over the period 24 August to 2 October 1987 at the ICRISAT Sahelian Centre in Niger, W. Africa. During this period, various small but fundamental investigations were conducted into the surface temperature characteristics of a millet crop, and measurements were made of complementary parameters associated with the separate soil and plant components.

This work provides a theoretical and experimental framework from which to design future experiments to measure the areal average surface temperature of a complex crop. Valid measurements are presented for soil and plant structure parameters but in view of the small scale sampling which was limited by the available instrumentation, this study does not yield accurate measurements of average surface temperature for a sparse millet crop.

Contents

1. Introduction

During the early stages of growth, most agricultural crops do not completely obscure the underlying soil surface when viewed from above. Millet, particularly when grown on poor soils in the tropics, remains sparse throughout its growing season, leaving a large proportion of the soil exposed which therefore contributes significantly to the overall micrometeorology of the crop.

When monitored by nadir viewing instruments, such as those commonly used in remote sensing, sparse crops present a complex surface of vegetation and soil each with contrasting surface characteristics, yet the instrumentation can only record a single spatial value to represent the integrated surface properties. It is therefore necessary to understand the component processes of a composite surface if remotely sensed data are to be used as input to physically based models of land surface processes.

One of the principal measurements included in remotely sensed multispectral data is land surface temperature. In the first instance, surface temperature data provide a measure of long-wave energy loss from the land surface: a component of the surface energy budget. Secondly, considerable research is being devoted to estimating regional evaporation using remotely sensed surface temperature. Clearly, it is necessary to understand composite surface processes if bulked pixel information is to be interpreted.

The principal instrument used in this study is the infrared thermometer (IRT) which records an apparent surface temperature based upon the long-wave radiational energy received in the 8μ - 14μ spectral band-pass. The narrow focus of each sensor allows surface temperature studies of the individual surface components.

This study, being very much a 'first-look', addresses the following crop and soil phenomena chosen as being relevant to the long-wave emission characteristics of a sparse millet crop:

- Percentage ground cover and its change with time
- Millet crop architecture with respect to emitted radiation
- Leaf emissivity
- Leaf surface temperature changes in space and time
- The measurement of soil emissivity
- The change in soil emissivity with respect to soil moisture
- Soil surface temperature changes in space and time
- The effect on surface temperature of soil surface structure
- Shading of the crop and soil surface by the crop elements
- The interpretation of the composite radiation sensed by an IRT mounted above the complex crop surface.

The study also gives an insight into the performance of infrared thermometers and soil thermistors in a semi-arid climate.

2. Instrumentation

2.1 OVERVIEW

The principal field instruments were two infrared thermometers (IRTs) made by 'Everest'. Each sensor head was mounted on a tripod of variable height to look down vertically at the soil and/or crop. In addition a hand-held IRT, made by 'Mikron', was available for check measurements of soil and leaf temperature. Soil temperatures were investigated with an array of bead thermistors (Figure 1). The output from the Everest IRTs and the thermistors was monitored by an Institute of Hydrology (IH) Epson interface and recorded on micro-cassette by an Epson HX-20 microcomputer. Standard IH software was used to control the data logging.

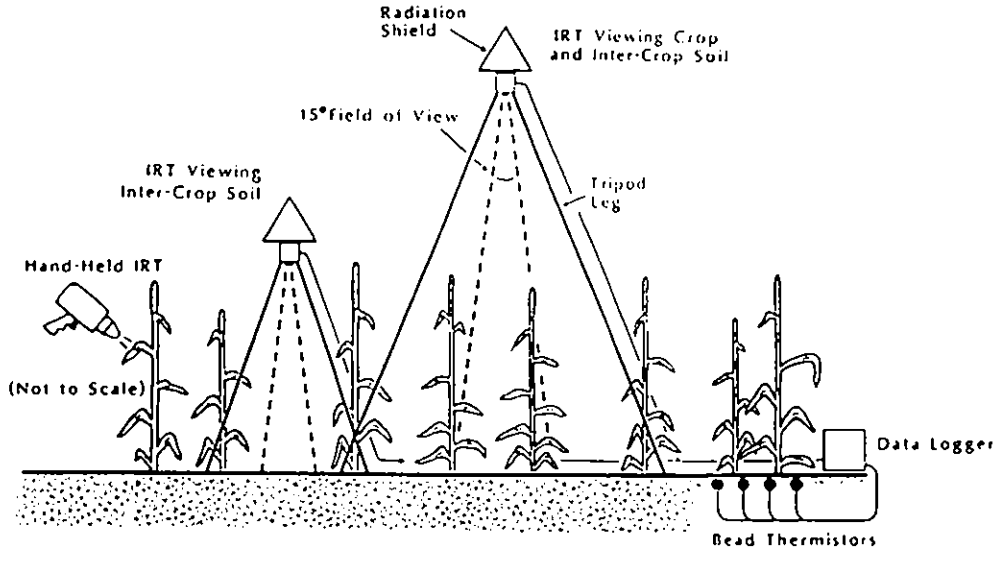

Figure 1 Arrangement of instruments

2.2 EVEREST INFRARED THERMOMETERS

The Everest IRT system uses two model 4000 transducer heads with 8μ to 14μ spectral filters, connected to a single multiplexer box. The multiplexer provides a display of the surface temperature of each transducer (assuming unity emissivity) and a millivolt output at 10.0 $mV°C^{-1}$. The field of view is a 0.218 steradian solid angle (15° included angle) giving a viewed circle diameter of 1.05 m at a distance of 4 m.

Before the field visit to the ICRISAT Sahelian Centre, the two Everest IRTs were calibrated at room temperature over a stirred water bath. The water temperature was varied from 20 - 60°C and was monitored by thermistors and

a mercury-in-glass thermometer. The IRT temperatures were mostly within 1°C of those indicated by the thermistors with some variation in gradient which, in hindsight, may have been due to the changing temperature of the instrument body. Calibrations between 40°C and 60°C were hindered by water condensing on the (cooler) instrument window. This was alleviated by laying a sheet of thin polythene on the surface of the water, allowing the thermistors to rest against the underside of the polythene to give the best estimate of surface temperature. Figure 2 shows the calibration of one of the Everest IRTs including the deviations due to condensation. In the field the multiplexer was kept from direct sunlight although no significant temperature sensitivity was found in its output when tested in an environment chamber to a temperature of 50°C.

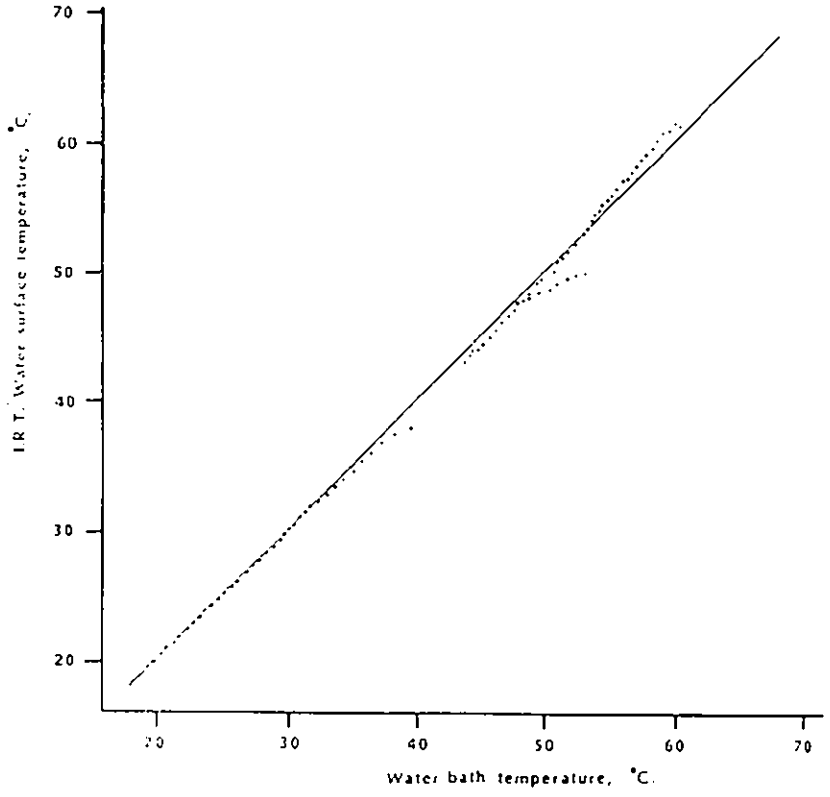

Figure 2 Typical calibration curve for an Everest IRT transducer showing deviations due to condensation of water on the transducer window

Since the field experiment, trials in an environment chamber have shown that the Everest IRTs retained a good calibration at constant temperature, but when the instrument is heating or cooling the indicated temperature is in error by 0.35°C for every °C h^{-1} in temperature gradient experienced by the sensor head (Wright, 1990). The temperature of the instrument body was not recorded in the field and it is not possible to compensate for changing body temperature without the necessary detailed information. This precludes accurate estimates of soil and leaf surface temperature and limits the use of the data to mainly comparative analysis.

2.3 MIKRON (HAND-HELD) INFRARED THERMOMETER

The Mikron IRT is a gun-like instrument which measures the temperature of the surface at which it is aimed. Small areas of a few square centimetres can be sampled at very close range, and the wide viewing angle allows the sampling of larger areas at relatively close range: 0.416 steradians (40° included angle) giving a viewed circle diameter of 0.73 m at a distance of 1 m. The instrument self-calibrates while switched on and displays the temperature when activated by a trigger.

As with the Everest IRTs the indicated surface temperature is sensitive to the instrument body temperature, but in addition the temperature regime during self-calibration is also important (see author's calibration notes Appendix 1). The instrument body temperature was not monitored in the field but the instrument was kept in the shade and air temperature recorded by an automatic weather station has been used as a substitute to correct the displayed readings. Reasonable results were obtained which are not thought to be more than 2°C in error considering the temperatures experienced by the instrument in the field.

2.4 THERMISTORS

Eight bead thermistors were available for burying close to the soil surface. Notwithstanding the acknowledged inadequacies of contact thermometry for estimating surface temperatures, the accuracy and reliability of these transducers was considered a worthwhile supplement to the experiments. The thermistors were 5 kΩ 'unicurve' bead transducers of about 1 mm in diameter and were powered from the 7.928 volt stable supply within the Epson logger interface. When connected into a high stability potential divider the thermistors gave a millivolt range suitable for the Epson interface (0.25 mV per logger step) and the expected climate of Niger.

At 0.25 mV per logger step (LS) the resistance, R, of the thermistor is given by:

$$R = \frac{25{,}000\ LS}{7.928 - 0.25\ LS} \quad \text{ohms} \qquad (1)$$

which can be used in the thermistor equation to give the temperature, T:

$$T = [8.0 \times 10^{-4} + 3.0 \times 10^{-4}\ \log_e R]^{-1} \quad K \qquad (2)$$

The resultant sensitivity is 0.049°C LS^{-1} at 50°C and 0.015 °C LS^{-1} at 20°C.

2.5 THE LOGGING SYSTEM

An Epson HX-20 was used as the controlling and logging processor for

synchronous recording of thermistor and Everest IRT temperatures. Flexible software, which facilitated 1, 5, 15 and 60 minute averaging of data over an instrument interrogation frequency of approximately two seconds, was provided by IH. The time, date, scan frequency and averaged temperatures were recorded on micro-cassette. All the temperature sensors were interfaced to the Epson HX-20 via an interface designed and constructed at IH.

The complete logger system (Epson HX-20 and interface) was tested for sensitivity to temperature and no significant drift was observed up to a maximum of 46°C. Operation of the Epson HX-20 is not recommended above a temperature of 50°C. Power for the installation was provided by a 12 volt lead-acid battery, which was more than adequate for keeping the system running for at least three weeks. The main inadequacy of the system was the net drain on the internal battery within the Epson HX-20, causing this small battery to be exhausted after seven days. The net drain is caused by the rate of supply from the lead-acid battery being limited to prevent damage by overcharging while the system is idle.

3. Theoretical long-wave radiation regime of a sparse crop

With reference to Figure 3 the radiation regime of a sparse crop can be seen as the direct and reflected components of the radiation from the crop, the soil and the sky. Although the long-wave component of radiation from the atmospheric gasses can be significant, this component is small in comparison with other emissions after reflection at the crop and soil surface and is not included in the following analysis. Multiple reflections and all reflections from the crop surface have been ignored due to the very low reflectance of the crop, $1 - \epsilon_c = 0.005$

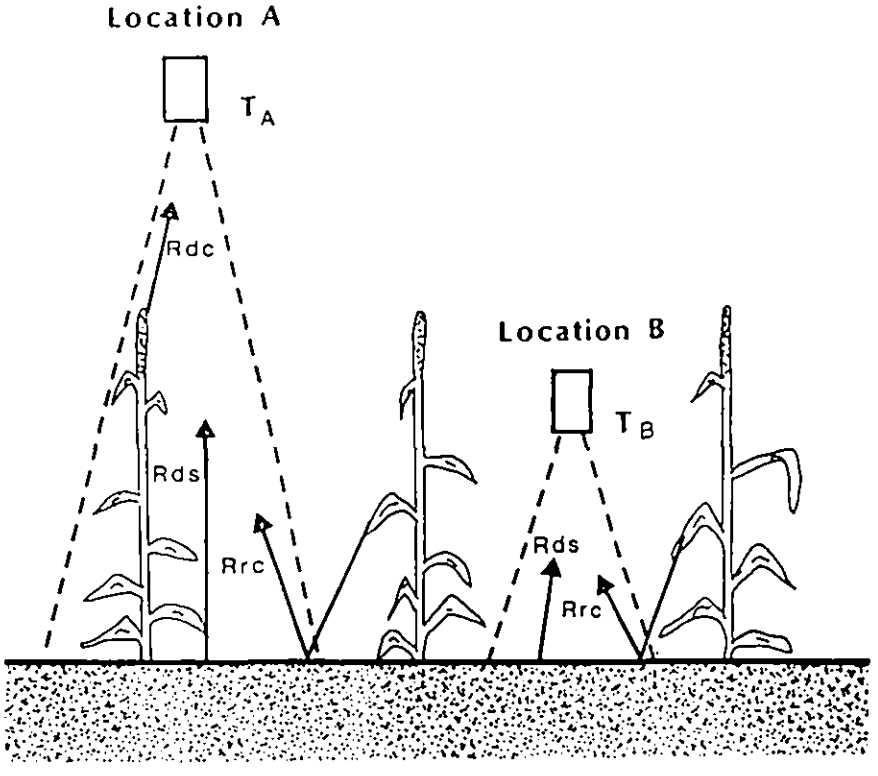

Figure 3 Principal components of the infrared radiation regime of a sparse millet crop

The remaining components can be parameterised as follows:

direct radiation from the crop

$$R_{dc} = \epsilon_c \sigma T_c^4 \qquad (3)$$

direct radiation from the soil

$$R_{ds} = \epsilon_s \sigma T_s^4 \quad (4)$$

and radiation from the crop reflected at the soil surface

$$R_{rc} = \epsilon_c \sigma T_c^4 (1 - \epsilon_s) 2\pi B \quad (5)$$

where R is radiation in Wm^{-2}
- ϵ is emissivity
- σ is the Stefan-Boltzmann Constant, = 5.67×10^{-8} $Wm^{-2}K^{-4}$
- T is temperature in K
- B is a crop structure parameter (see Section 4.1.2)

and the suffixes refer as follows:
- d to direct radiation
- r to reflected radiation
- s the soil surface
- c the crop surface.

The effective temperature of a composite surface, as indicated by an IRT, will be the sum of the various components multiplied by their respective areas. Therefore, an IRT viewing a crop and soil composite (position A in Fig. 3) will indicate an effective temperature T_A, given by:

$$\sigma T_A^4 = R_{dc}(1-p) + R_{ds}p + R_{rc}p \quad (6)$$

where p is the proportion of plan area that is soil.

Substituting into Equation 6 from Equations 3, 4 and 5 and dividing by σ gives:

$$T_A^4 = \epsilon_c T_c^4(1-p) + \epsilon_s T_s^4 p + \epsilon_c T_c^4(1-\epsilon_s)2\pi Bp \quad (7)$$

Similarly an IRT viewing inter-crop soil (location B in Fig. 3) will indicate a temperature, T_B, given by:

$$\sigma T_B^4 = R_{ds} + R_{rc} \quad (8)$$

Substituting into Equation 8 from Equations 4 and 5 and dividing by σ gives:

$$T_B^4 = \epsilon_s T_s^4 + \epsilon_c T_c^4 (1-\epsilon_s)2\pi B \quad (9)$$

Equations 7 and 9 can be solved to give the crop temperature

$$T_c = \left[\frac{T_A^4 - pT_B^4}{\epsilon_c(1-p)} \right]^{0.25} \quad (10)$$

which can be seen to be principally dependant on only the plan area parameter, p, and independent of the more sensitive parameters ϵ_s and B.

Also, equations 7 and 9 can be solved to give the soil temperature

$$T_s = \left[\frac{1}{\epsilon_s} \left[T_B^4 - \frac{T_A^4 - pT_B^4}{1-p} (1-\epsilon_s) 2\pi B \right] \right]^{0.25} \qquad (11)$$

4. Individual experiments

4.1 TO EVALUATE CROP ARCHITECTURAL PARAMETERS BY PHOTOGRAPHY

4.1.1 Plan area parameters looking vertically down

A vertical view of a crop will show not only the proportion of plan area occupied by crop and soil, but also the proportion of crop and soil in direct sunlight or shadow at specific times of day. All four of these surface types will have a different temperature associated with its surface energy balance as well as variations within each type due to differences of soil moisture, leaf age and status. The radiation received by an IRT will be a composite of all these temperatures and the evaluation of crop architectural parameters by vertical photography can help to interpret the effective temperature that is output by the sensor.

Fifty vertically downward photographs were taken over the millet crop at the ICRISAT Sahelian Centre, at different times of day and over points where an Everest IRT had been operated. The locations had been chosen to encompass a range of crop densities. All the photographs were taken during the period of intensive measurements, i.e. from the 54th to 61st day after crop emergence, with the exception of a single photograph taken on the 89th day, just before harvesting.

Of the 50 photographs, 38 were selected for analysis and projected onto a white card on which a square grid had been drawn. The proportions of plan area that were plant or soil and shade or direct sunlight were determined by the state indicated at each of the 260 grid intersections within a circle representing the field of view of the IRT.

Table 1 shows the range of values of p, the proportion of plan area that is soil. It should be noted that the sites were not randomly selected but chosen for their range of p values, and therefore the overall mean value has not been calculated. The individual p values for each site are used in Section 4.5 for comparison with IRT measurements over the same locations.

The diurnal variation of the proportion of vertically viewed crop and soil in shade is shown in Figures 4 and 5 respectively. As would be expected, the complex crop surface shows much more variation at a particular time compared to the planar soil surface. The proportion of soil shaded, as shown in Fig. 5 should not be confused with extinction coefficient (Wallace personal communication) which has a similar diurnal curve. Figure 5 excludes information about the part of the soil which is obscured from view by the crop and is only relevant to instruments mounted above the crop.

Evidence from Fig. 4 that the proportion of shaded crop is only weakly related to time of day and not less than 0.25, is used to justify the averaging of individually measured shade and sunlit leaf temperatures to give a bulked value of leaf surface temperature (Section 4.4.2).

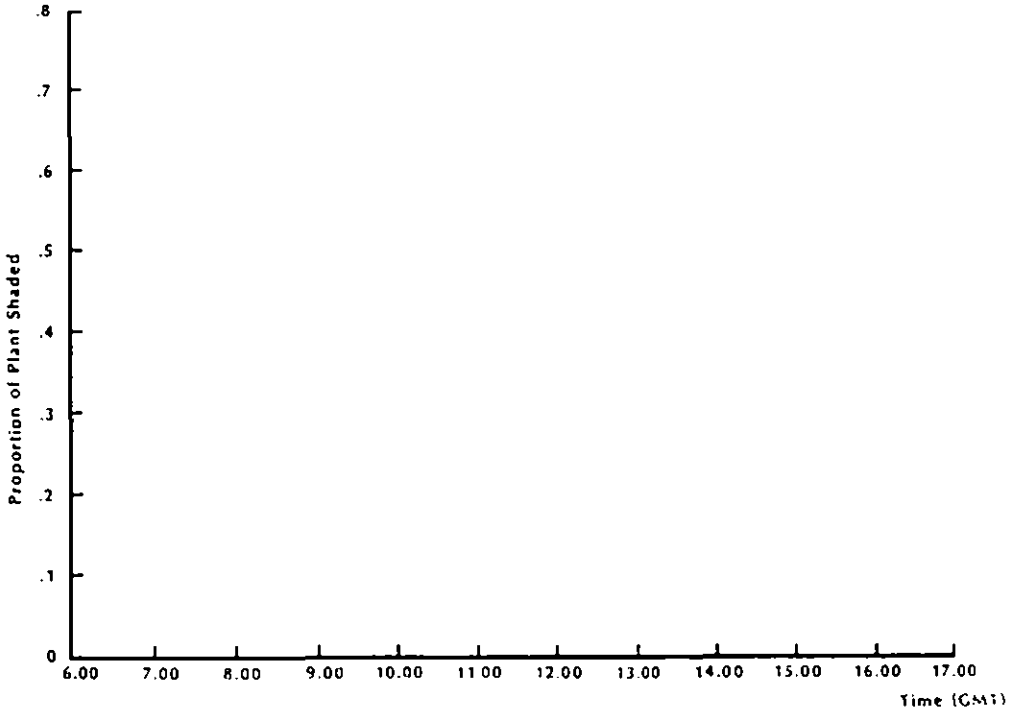

Figure 4 Diurnal variation of the proportion of crop plan area that is shaded

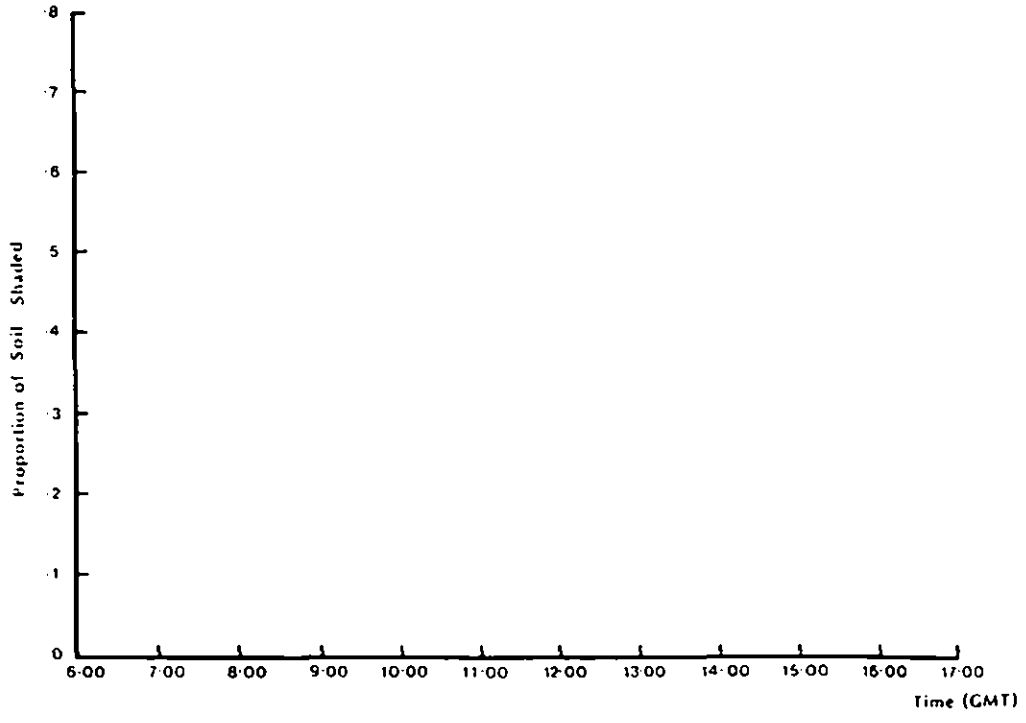

Figure 5 Diurnal variation of the proportion of soil plan area that is shaded

Table 1 Proportion of the plan area that is soil

Site	p	Standard deviation	No. of photographs
Centre	0.311	.013	7
A	0.306	.007	2
B	0.354	-	1
C	0.227	.003	14
D	0.244	.020	3
E	0.259	.014	2
F	0.502	.008	2
G	0.238	.019	2
H	0.259	.013	2
I	0.444	.017	2
pre-harvest	0.449		

Although these data are specifically related to this crop and its particular height, spacing, health and stage of development, the result shows a simple method of evaluating specific architectural parameters for which the theory of Ross (1981) can provide only a statistically general result.

4.1.2 Radiation penetration function

The radiation penetration function, a_d, is the proportion of sky hemisphere, at a given zenith angle, visible at a given depth within a crop stand. This is an important parameter when considering the radiation energy received at the ground from the crop or the sky. In the case of infrared radiation received at a point from the surrounding crop stand, it is not sufficient to integrate this function to provide a single value with which to multiply the radiation associated with the crop temperature. The radiation received from the crop is also related to zenith angle by Lambert's Cosine Law and must be combined with the penetration function before integration to give the energy received per unit soil surface area.

Thus if the penetration function, a_d, (Ross, 1981), which is equivalent to the proportion of sky visible from the soil surface, for radiation at zenith angle ϕ, into a crop of height L is given by:

$$a_d = f(\phi,L) \qquad (12)$$

and the radiation, dR, received by unit area of a planar surface from an annular portion of a hemispherical emitter of emittance N (see Appendix 2) is given by:

$$dR = 2\pi N \sin\phi \cos\phi \, d\phi \qquad (13)$$

Then the radiation, R, received at a planar soil surface from the non-homogeneous crop structure equals $2\pi N.B$

$$\text{where } B = \int_{\phi=0}^{\phi=\pi/2} \text{Sin}\phi\text{Cos}\phi(1\text{-f}(\phi,L))\ d\phi \qquad (14)$$

B represents the integrated proportion of radiation emitted by the crop structure and received at the soil surface. This integral can be solved when the penetration function is defined by architectural theory, photography or radiometry.

Figure 6 shows data extracted from the vertical photographs and three photographs taken from ground level within the millet crop. A similar transect method to that of Section 4.1.1. was used to determine the proportion of crop within equal ranges of zenith angle. Also shown are lines representing measurements taken at various depths in a maize crop (Ross, 1981). Although the planting density of the maize will be different from that of the millet, affecting the position of the curve relative to the measurement height the important result is that the shape of the curves is very similar to that of the measured data. Ross shows that the shape of the curves varies greatly with leaf shape and orientation.

In order to evaluate a value for the crop structure parameter, B, it is proposed that a simple function can be drawn to represent the penetration function of the millet crop. The function, which is shown as a dashed line in

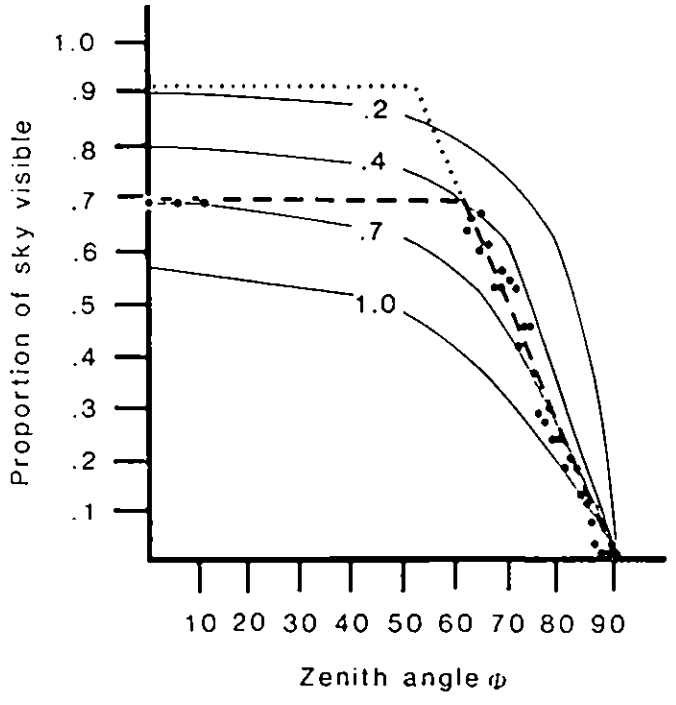

Figure 6 The proportion of sky area visible from the soil with respect to zenith angle, showing measured data from this study (●), from Ross, 1981 (——) and simple models for the purposes of integration (- - - and ·)

Fig. 6, has been chosen initially to intercept the ordinate at 0.69 or (1-0.31), the proportion of plan area that is crop (Section 4.1.1) at the central IRT installation point.

Integration of Equation 14 with substitution of the approximate penetration function (dashed lines in Fig. 6) derived for the millet crop yields a value of B = 0.183. Therefore the radiation received on unit area of soil from the millet crop at temperature, T, can be calculated as

$$2\pi . \epsilon_c \sigma T^4 . \ 0.183 \qquad (15)$$

Further experimental evidence for a value of B, the penetration function integrated with crop long-wave radiation, is given in Section 4.3.2.

4.2 SOIL CHARACTERISTICS AND MEASUREMENTS

4.2.1 Soil surface temperature measurement

Contact thermometry is acknowledged to be systematically in error when used to estimate surface temperatures. This will be particularly so in soils exposed to direct sunlight because of the large temperature gradients at the surface (Fuchs and Tanner, 1966). Nevertheless, the reliability, accuracy, cheapness and small physical size of bead thermistors are of great benefit towards providing a foundation measurement with which to compare other instruments and calculations of temperature.

A simple experiment was constructed in which both Everest IRTs were mounted at a height of one metre over clear plots of bare soil and within each field of view thermistors were buried at approximately 2 mm and 6 mm below the surface. Plot A contained soil which was undisturbed since recent rain and was capped by a weak crust (see Section 4.2.2 below) and Plot B contained soil which had been raked to destroy the crust.

Additionally, two experimental thermistors were laid on the soil surface in each plot having first been painted with matt yellow enamel and then coated in sand. The resultant permanent sand covering was intended to represent the smallest possible installation depth while being less easily disturbed by surface movement of the soil. The very friable nature of the sandy soil at the ICRISAT Sahelian Center precludes long-term installation of shallow thermistors because of surface disturbance by rain, wind and insects and it was necessary to re-install the shallowest thermistors at frequent intervals.

Figures 7 and 8 show the measured changes in temperature at 2 mm and 6 mm below the soil surface for plots B and A respectively. Also shown are the temperatures indicated by the IRTs, corrected for emissivity (ϵ_s = 0.916, see Section 4.2.3), and the experimentally coated thermistors. The downward dips in all the lines around midday are caused by the IRT shadow passing through the field of influence of the various sensors; this effect is much less significant to the IRT measurements when the instruments are raised to their full height.

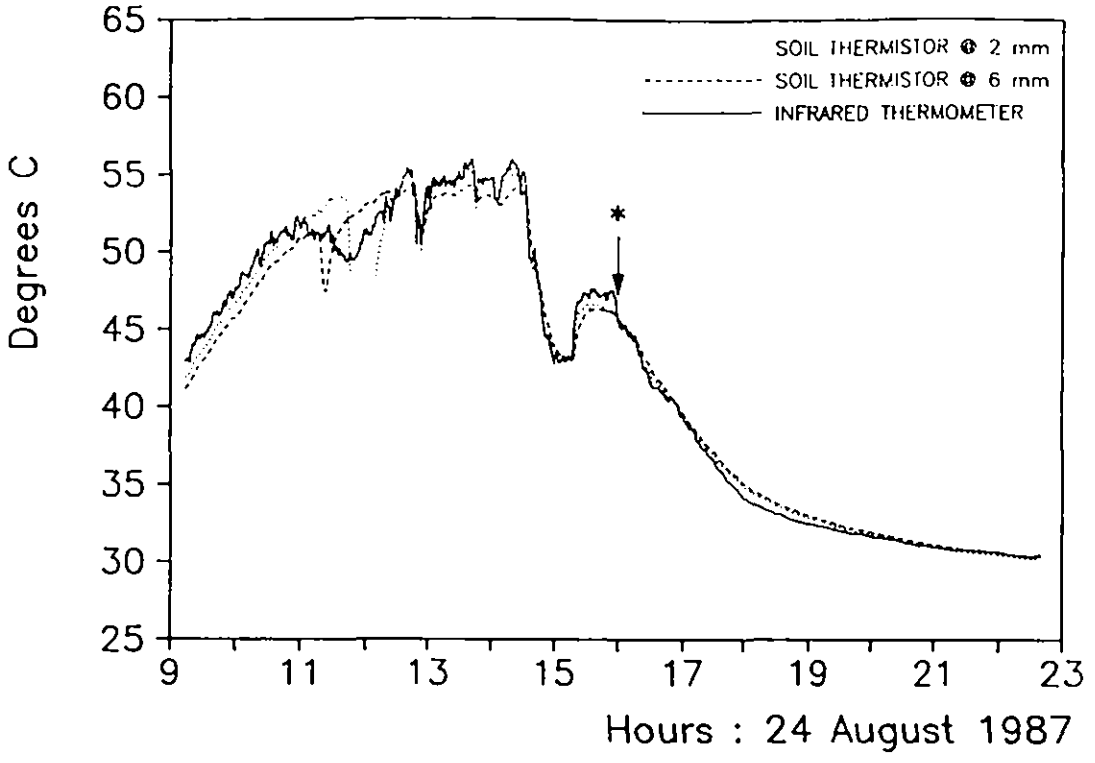

Figure 7 Infrared thermometer and thermistor temperature measurements of disturbed bare soil

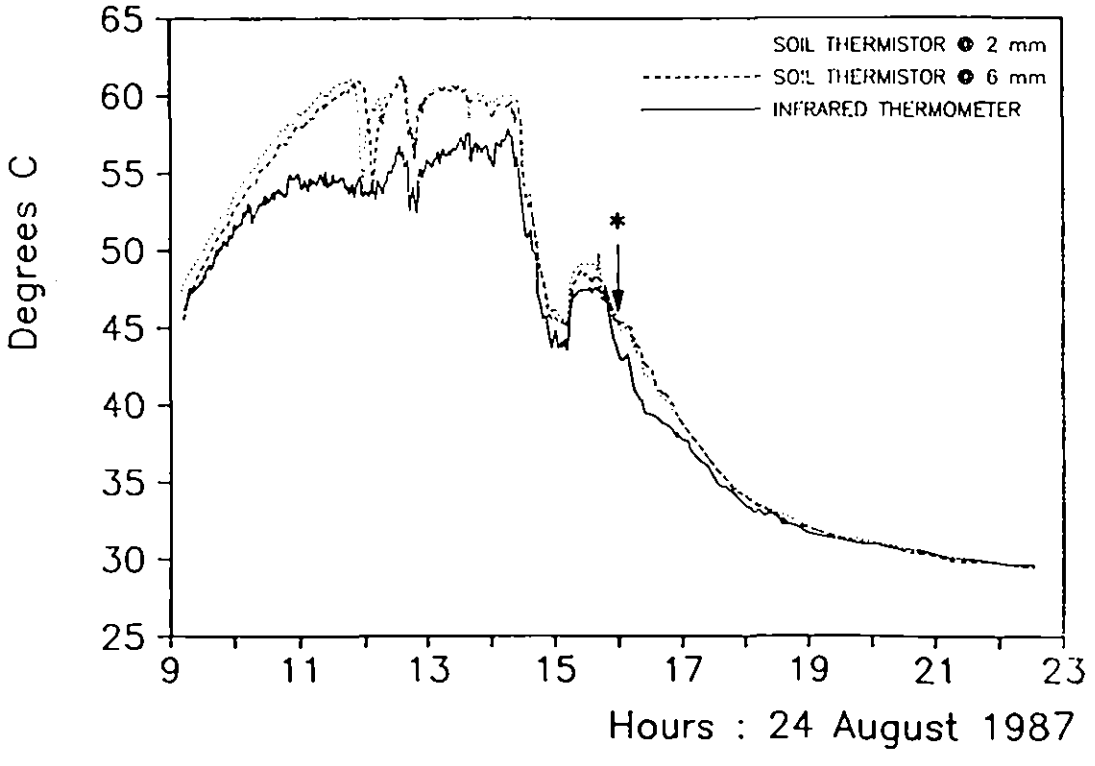

Figure 8 Infrared thermometer and thermistor temperature measurements of undisturbed bare soil

Figure 7, which illustrates surface temperatures associated with the soil with no surface capping, shows a misleadingly good performance for the IRT. This is because emissivity was evaluated from these data using the point in time indicated by an asterisk. The residual performance relative to the two thermistors is the combined effects of soil surface temperature gradients and air temperature on the IRT body (Section 2.2). Both of these effects will cause an overestimate of surface temperature during rising temperatures and an underestimate for falling temperatures.

Figure 8 shows a similar performance over the capped soil except that the IRT estimate of temperature is grossly in error through the middle of the day. There is no confirmable explanation of this result; an object that was cooler than the soil was possibly within the field of view: It was observed later that certain insects found the IRT orifice an ideal support for webs and cocoons. The experimentally coated thermistors performed very badly being excessively influenced by the air temperature.

Notwithstanding the limitations of this experiment, the response of the shallow thermistors relative to that of the IRTs indicates that the thermistors can be used as adequate estimates of soil surface temperature for some short-term experiments. As will be shown later (Section 4.3.1) soil surface variability can be far greater than the small systematic error introduced by using subsurface thermistors.

4.2.2 Soil surface capping

The soil at the ICRISAT Sahelian Centre (ISC) typically consists of 91% sand, 4% silt and 5% clay (West *et al.*, 1984). After rainfall the small clay fraction bonds the drying soil at the surface forming a crust of low mechanical strength, then as the soil continues to dry, the bonds become very weak and the surface capping reverts to a loose friable structure.

As mentioned in the previous Subsection (4.2.1) thermistors were installed within plots of capped and disturbed soil. Compared to Fig. 7, Fig. 8 shows the significantly warmer temperatures associated with the capped soil which would be expected from the impeded ventilation and reduced evaporation through the capping.

4.2.3 Dry soil emissivity

An initial attempt was made to measure the emissivity of the dry soil surface using a method described by Fuchs and Tanner (1966) where an internally reflective cone is placed over the surface forming a 'black' cavity which can be viewed by an IRT from a hole at the apex of the cone. The emissivity of the surface is determined from the IRT temperatures that are measured with and without the cone in place.

At the ISC the Mikron hand-held IRT was used with two 100 mm high cones made from stiff paper with the inner surface made reflective with either aluminium foil or aluminised plastic. Emissivities calculated using this method

were very variable, ranging from 0.95 to 0.98, and are significantly greater than those quoted in previous work (see Table 2). It is unlikely that these values are a satisfactory measurement of emissivity as the method appears very sensitive to experimental design and the cones used at ISC were probably too small and the inner surface insufficiently reflective to thermal radiation to create the required 'black body' cavity.

Table 2 Values of emissivity from previous work

Source	Soil		Emissivity
Fuchs and Tanner (1967)	Plainfield sand		0.900 ± 0.001
Buettner and Kern (1965)	Quartz sand large grain		0.914
	Quartz sand small grain		0.928
		Mean	0.914

Further investigations of emissivity were undertaken in the evening when temperature gradients in the top few millimetres of the soil are minimal and when infrared radiation from a cloudless sky is not significant in the 8-14 μ bandpass. Under these circumstances, thermistors placed near the surface of the soil will give a reasonable estimate of soil surface temperature due to the neutral temperature gradients at the surface. The reinversion of surface temperature gradient which occurs in the morning is more difficult to utilize as the surface temperature changes more rapidly at this time compared with evening inversion. For a dry sandy soil, the difference between the apparent temperature indicated by an IRT and the real surface temperature will be principally due to surface emissivity, assuming that there are no nearby radiating objects significantly obscuring the sky hemisphere.

If temperatures at two depths are available, the optimum time for emissivity measurements is at the end of a day, immediately before the vertical temperature gradient is seen to invert. At this moment the shallower thermistor will indicate the best estimate of true surface temperature.

In the experiment over bare soil described above (Section 4.2.1), the soil thermistors in each plot showed a clear inversion point (marked by an asterisk in Figs. 7 and 8). Temperatures from the two 2 mm thermistors and the two IRTs were averaged over the 10 minutes preceding the inversion time and gave emissivities of 0.907 and 0.924 for the capped and disturbed soil respectively. These values agree favourably with those quoted in the literature (Table 2), although the absence of a correction for sky radiation will tend to make these values systematically high.

The mean of the two calculated emissivities, 0.916, will be used in all following calculations as the inter-crop soil has a surface structure which is only partially capped where it has remained undisturbed by human, animal and insect activity.

4.2.4 Effects of surface soil moisture

The emissivity of a sandy soil surface will be affected by moisture content as the emissivity of water (ϵ_w = 1.0) is significantly different from that of the dry sand. Evaluation of this phenomenon is not easy as the moisture content of a surface is difficult to define. It is necessary to assume that the moisture content at the surface is represented by the moisture content of a thin layer carefully sampled from the surface of the soil (Fuchs and Tanner, 1968).

A simple experiment was constructed using the Everest IRTs over a soil which was well saturated from overnight rain. Four shallow thermistors were used to give an estimate of the soil surface temperature and, during the day as the soil dried naturally in the sun, 22 soil samples were collected from the top 10 mm of soil. Their relationship is shown in Figure 9.

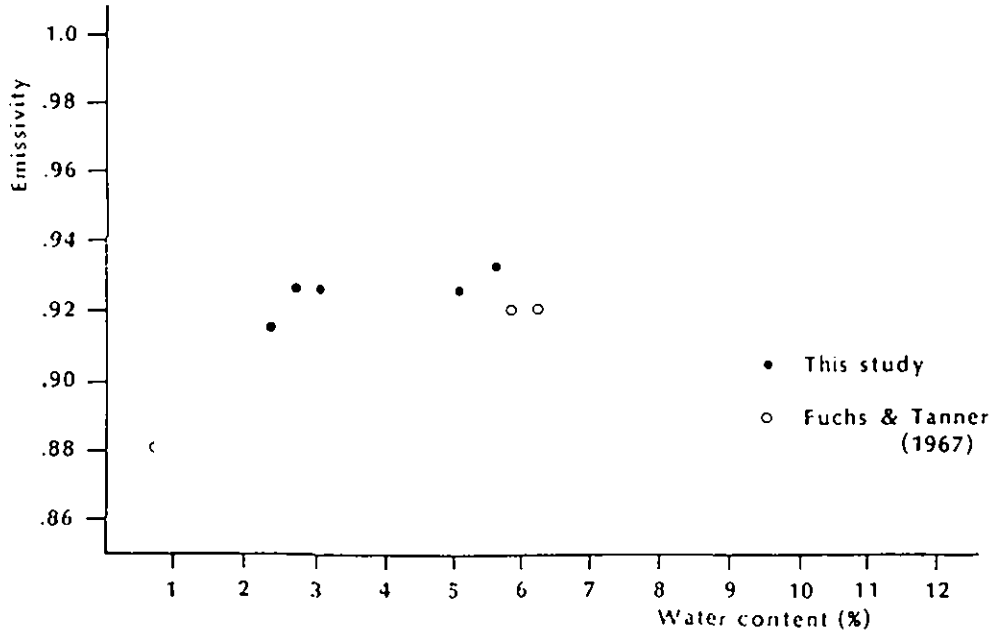

Figure 9 Emissivity of a bare soil surface plotted against percentage soil moisture

A systematic error will be introduced by reflectance of sky radiation at the soil surface and by the soil thermistors which underestimate the surface temperature, both effects result in an overestimate of emissivity. Also, the relatively small number of soil samples will introduce a random error.

Notwithstanding these errors, the resultant relationship between emissivity and moisture content agrees well with data published by Fuchs and Tanner. It should be noted that the moisture contents evaluated by Fuchs and Tanner will be systematically higher than those measured at ISC as the former study took samples from the top 25 mm of soil.

4.3 INTER-CROP SOIL SURFACE TEMPERATURE MEASUREMENTS

4.3.1 Thermistor soil temperatures

Thermistors placed carefully just under a bare soil surface have been shown to give an indication of the surface temperature (Section 4.2.1). Figure 10 shows that four thermistors installed in a similar manner within a crop stand give widely varying temperatures both in time and space. Much of this variation will be caused by their position relative to the ridging of the soil, the plants and the passing of the plants' shadows. The agreement between thermistors at night indicates the absence of instrumental errors other than possible placement errors caused by soil disturbance.

The mean value for the four thermistors is used for subsequent comparison in the following sections even though the standard error of the mean temperature may be as high as 3 or 4°C.

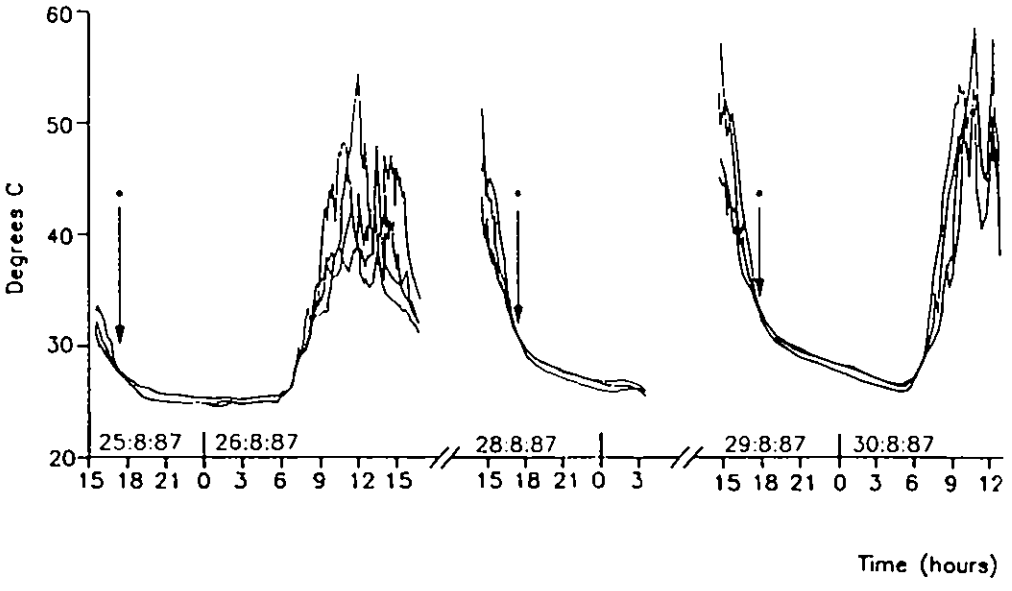

Figure 10 Soil surface temperatures within a crop of millet plotted against time.

4.3.2 Everest IRT soil temperatures

In an attempt to verify the theoretical radiation regime outlined in Section 3, the two Everest IRTs were erected in the millet crop with one sensor at 4.0 metres looking down at the composite soil and plant surface, and the other sensor mounted at 1.8 metres, the highest possible location that would view a maximum area of inter-crop soil but without seeing any of the crop (Fig. 1). Four thermistors were installed close to the soil surface to give an estimate of the soil surface temperature for comparison with those calculated from Equation 11.

An experimentally derived value of the integrated penetration function was calculated from three clearly defined surface temperature inversions observed in the data (described in Section 4.2.3). Assuming that the temperature of the crop is the same as that of the soil in these conditions (in all three cases the two IRTs were consistently less than 0.4°C different), Equation 9 can be rearranged to give:

$$B = \frac{T_B^4 - \epsilon_s T_s^4}{2\pi \epsilon_c (1-\epsilon_s) T_c^4} \qquad (16)$$

The three values calculated from Equation 16 where B = 0.116, 0.115 and 0.112, which are significantly lower than the value of B = 0.183 obtained by photography. An explanation of this difference may be considered by reference to Fig. 6. The mean penetration function calculated from Equation 16, B = 0.114, is equivalent to the integration of the straight line function but with the horizontal portion intercepting the ordinate at a value of 0.91, (p = 0.09, shown by the dotted line), instead of the photographic value 0.69 (p = 0.31, shown by the dashed line). It is reasonable to suggest that the experimentally derived value is smaller than that derived from photography because the regions of soil viewed by the higher IRT are logically those that have no elements of crop vertically above them: an important consideration when comparing nadir viewing instruments with other experimental techniques.

Figure 11 shows some of the Everest IRT data after substitution into Equation 11 to give an estimate of soil temperature. The parameter values used were ϵ_s = 0.916, p = 0.3, and B = 0.114. Also shown are the mean temperature indicated by the four soil thermistors and the temperature of the lower IRT divided by the soil emissivity, $T_B \epsilon_s^{-1}$ which, for comparison, is an estimate of inter-crop soil surface temperature which would result if the phenomenon of soil reflectance were ignored.

It can be seen in Fig. 11 that the inadequately sampled surface temperature data as measured by the thermistors are not sufficient to discriminate between the two IRT estimates of surface temperature which either include or exclude the effects of soil surface reflectance. Although the agreement between the thermistors and IRTs at night is dominated by the value of B optimised on these data, the results show that, if the chosen parameters are correct, the reflectance of crop radiation at the soil surface can affect the temperature indicated by an IRT by a significant and systematic amount throughout the day.

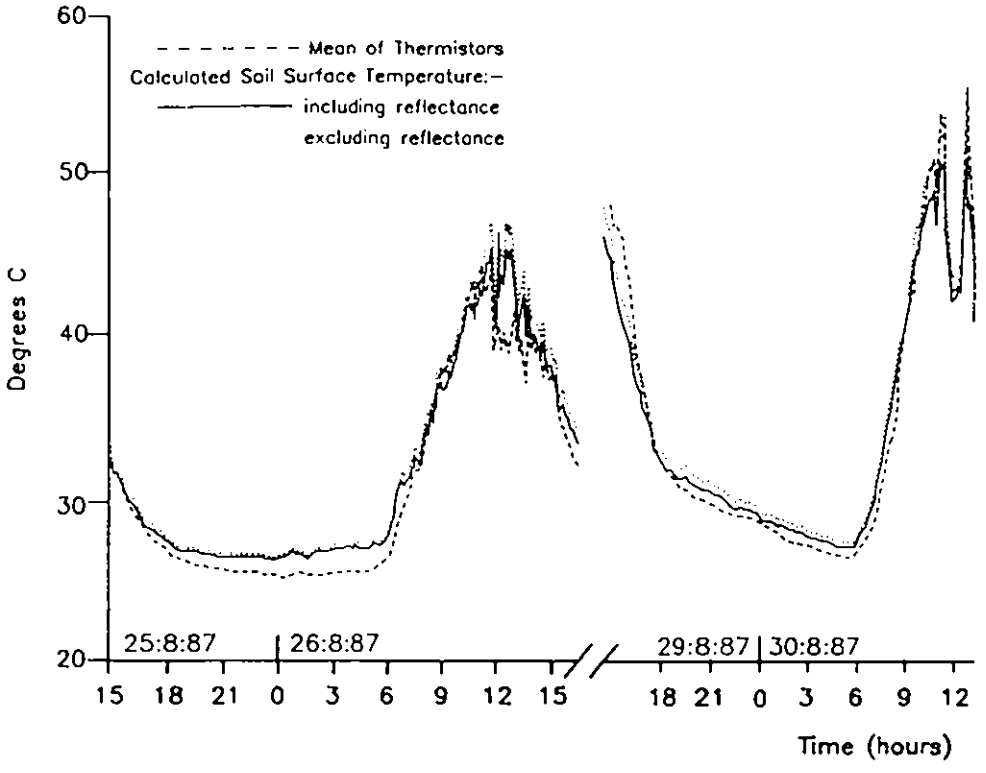

Figure 11 Mean soil surface temperature within a crop of millet plotted against time including IRT estimates of surface temperature with, and without, the effects of soil surface reflectance

4.4 LEAF TEMPERATURE MEASUREMENTS

4.4.1 Leaf emissivity

No attempt was made to measure the millet leaf emissivity in the field. The available instrumentation would not have been adequate for a reliable measurement of leaf surface temperature. Also, no published values of millet leaf emissivity have been found. Idso *et al.* (1969) give emissivity values for 34 different species of plants ranging from 0.938 to 0.995 in which only two monocotyledons are included: maize (ϵ_c = 0.944) and sugar cane (ϵ_c = 0.995). The value of 0.995 was chosen to represent the millet on the subjective grounds that sugar cane has the more similar leaf (J. Roberts, personal communication).

4.4.2 Mikron IRT leaf temperatures

The Mikron hand-held IRT was used to survey leaf surface temperatures for comparison with those calculated from the Everest IRTs. Each survey consisted of temperature measurements from all the leaves of five plants with separate measurements of sunny and shaded portions of leaf when available. A total of 21 surveys were conducted: six surveys at two-hourly intervals on each of 26 August, 2 September and 30 September, two surveys on the afternoon of 28 August and one on the following morning.

Results from the six surveys of 26 August are shown in Figure 12, each line representing the mean of five plants. The figure shows that the location of shaded leaves is only weakly dependent on leaf number, i.e., the height of the leaf from the ground. Also, from Section 4.1.1, the proportion of plan area which is shaded leaves is only weakly dependent upon the time of day. Therefore, it is considered reasonable to bulk the Mikron IRT leaf temperature measurements from all heights and over the duration of an hour for comparison with those from the Everest IRT.

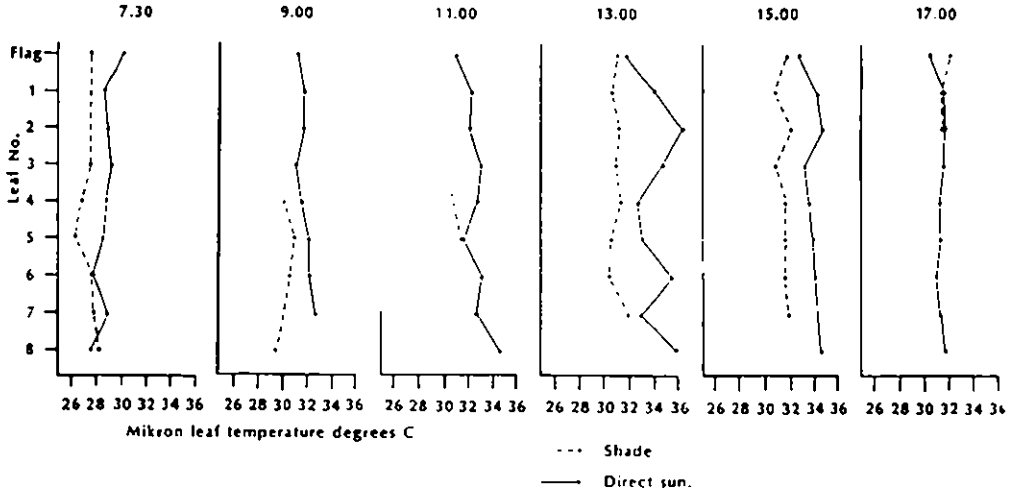

Figure 12 Leaf temperature profiles within a crop of millet

Further points of interest shown in Fig. 12 are as follows:

1. Negative gradients of temperature from the flag leaf to leaf two, during most of the day, indicate the ability of the flag leaf (and to some extent leaf one) to continue transpiring, while lower leaves are responding to stress and becoming warmer due to reduced transpiration. The lower leaves will also be affected by reduced ventilation and therefore higher temperatures.

2. Large negative gradients at the bottom of the profile indicate the onset of senescence in the lowest leaves.

3. The last profile shows that the flag leaf shade temperature is higher than the temperature in direct sun light. This shows the stimulation of stomatal opening by very low levels of irradiance and the resultant transpiration cools the leaf, there being insufficient energy in the radiation to satisfy the latent heat demand.

4.4.3 Everest IRT leaf temperatures

Data from the Everest IRTs, with the instruments arranged in the manner of Fig. 1, were substituted into Equation 11 to give crop surface temperatures to coincide with those surveyed with the Mikron hand-held IRT. Figure 13 shows the resultant poor agreement between the estimates of crop surface temperature from the two non-contact methods.

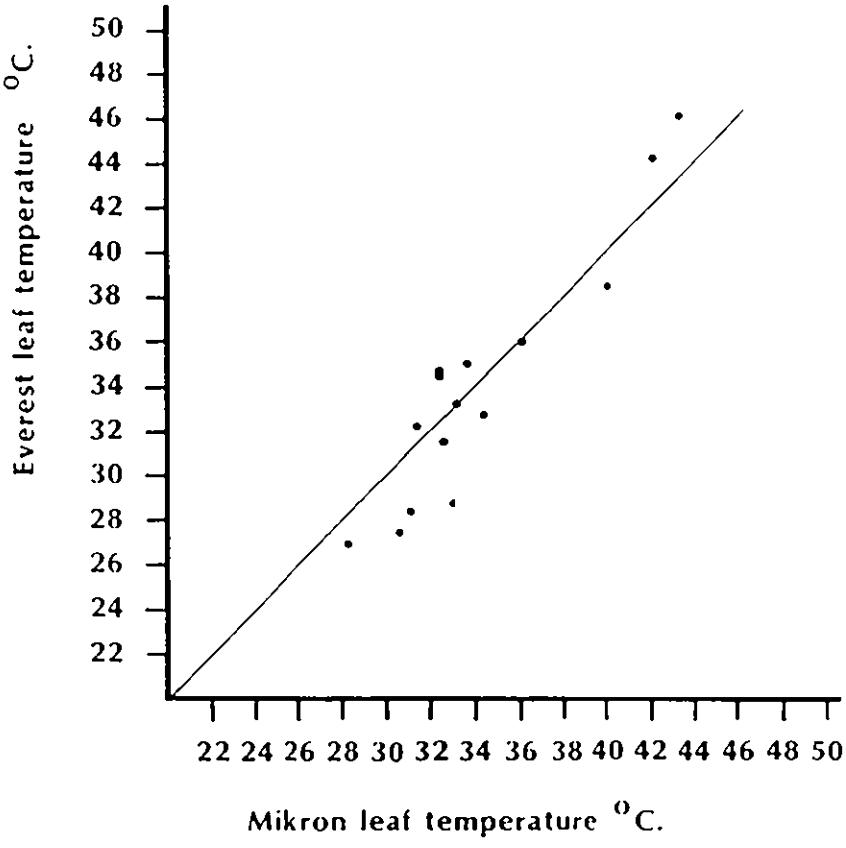

Figure 13 Comparison between leaf surface temperatures as measured by the 'Everest' and 'Mikron' infrared thermometers

Considering the encouraging results from the two independent methods of measurement, it is not easy to understand the reasons for, and the magnitude of, the discrepancy. Although the exact calibration of the instruments has not been possible and the theoretical calculations are sensitive to some parameters, the disagreement is beyond the limits that might be expected from calibration errors. Also the parameter distortion required to account for the

disagreement takes the parameters to values outside reasonable limits. The only physical explanation for the disagreement is a substantial spatial variation, possibly in the leaf temperature but more likely in the soil surface temperatures. A better result may have been achieved if the lower IRT had viewed an area of soil within the field of view of the higher IRT viewing the crop/soil composite.

4.5 SPATIAL VARIATION OF AREAL RADIATION

The spatial variation of radiation from the crop/soil composite was investigated using both Everest IRTs to look at the crop from the same height (4 m), leaving one IRT at a fixed position while the other IRT was moved to surrounding locations. Due to limitations in the cable lengths it was not possible to sample a representative foliage density. Therefore, locations were chosen to encompass the available range of densities so that at least the effect of foliage density could be observed. For each pair of locations data were recorded for a minimum of 2.5 hours. At each location nadir viewing photographs were taken to measure the proportion of plan area which was soil, p (see Section 4.1.1).

The results showed a complete absence of correlation between the amount of radiation emitted by the crop/soil composite and the proportion of soil viewed. Therefore, within the range of p values measured (0.227 to 0.502), spatial variation in crop and soil temperatures appears to dominate the total emittance: a similar conclusion to that of the previous section.

4.6 TEMPORAL VARIATION OF AREAL RADIATION

After the period of intensive field measurements the two Everest IRTs remained in the crop for a further 30 days and configured as shown in Fig. 1. During this period 23 days of 5 minutes data were recorded at 5 minute intervals on 23 of the days, monitoring soil and crop/soil temperatures to within a few days of harvest. No thermistors were installed as they would have become uncovered during rainfall.

In view of the poor results in estimating crop temperature (Section 4.4.3), these data, which have no means of absolute verification, have not been substituted into Equation 11 to give a longer run of estimated crop surface temperature. Instead, the data have been used comparatively to show the change in structure of the millet crop throughout the period of measurement.

As the leaves age, becoming more inefficient and ultimately dying, they transpire less and their temperature will rise. Also, as the leaves wilt their plan projected area will decrease as can be seen in Table 1 ($p = 0.311$ to $p = 0.449$ for the central plot). Therefore, the difference in long-wave emission between the inter-crop soil and the crop/soil composite will decrease.

Figure 14 shows the effect of crop senescence expressed as the diurnal

amplitude ratio of the two Everest IRTs for all available data. With time, the ratio approaches unity as the influence of the transpiring crop diminishes. It can be seen from the available data that throughout the last half of the millet crop's life the composite surface temperature of the sparse crop is increasingly influenced by the temperature of the underlying soil.

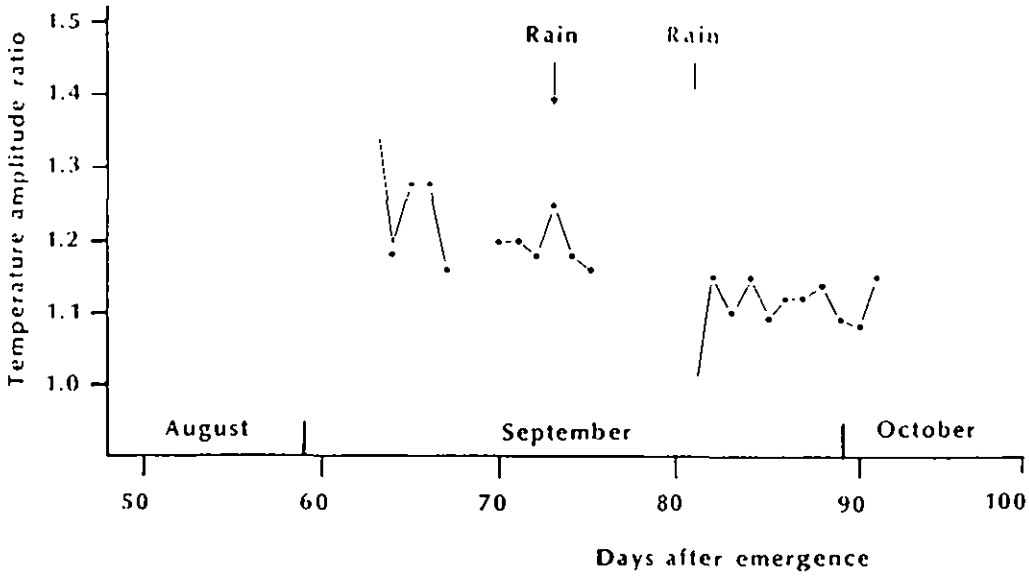

Figure 14 The ratio of soil to soil/crop diurnal temperature amplitude plotted against time showing the change in crop structure throughout the measurement period

5. Conclusions

Current instrumentation for the measurement of surface temperature by sensing infrared emission is particularly difficult to calibrate and notoriously sensitive to the working environment (Kalma *et al.*, 1988; Huband, 1985; Fuchs and Tanner, 1966). It is unfortunate that calibration of the instruments used in this study was not possible before deployment in the field. Both the Everest and Mikron instruments were found to be seriously sensitive to their own body temperature. In the case of the Mikron IRT the instructions imply that it was designed for use at room temperatures rather than in the hot climate of Niger.

Subsequent work has shown that instrument body temperature correction will improve the absolute accuracy of both types of IRT (see Appendix 1 and Wright, 1990).

The results from this pilot study into infrared thermometry at the ICRISAT Sahelian Centre, while being poor in accuracy, show that each instrument is consistent within itself and have yielded the following useful information about the soil and crop.

- Both soil surface moisture and soil surface structure affect the energy balance at the soil surface by changing its emissivity and porosity to water vapour.
- Acceptable values of soil emissivity and B, the crop structure parameter, were derived from times of neutral temperature when the soil, crop and IRT's were all at similar temperatures.
- Leaf temperature and leaf shading were found to be only weakly dependent upon height within this type of sparse crop stand.
- Throughout the last 40 days of the crop season the surface temperature of the soil/crop composite was increasingly influenced by the underlying soil temperature.

If the parameters values used in the theory are correct, then this work indicates the importance of the reflectance of long-wave radiation at the soil surface from the surrounding crop. The additional emittance from the soil increases the apparent soil surface temperature by a significant and systematic amount throughout the day.

Unfortunately, it was not possible to sample adequately the extreme variability of the surface temperature of the intercrop soil but only to acknowledge its effect. With only two logged IRTs at limited fixed positions all attempts to observe the effect of crop surface temperature upon the composite soil/crop emittance were obscured by the variability in the dominant soil component. Also the poorly sampled intercrop soil temperature precluded the absolute verification of soil surface reflectance.

In conclusion, this study has been an initial investigation into the complex field radiation regime and its accompanying theory, both of which can usefully be improved. These improvements are necessary if remotely sensed data are to be interpreted with respect to the water and energy balance of this type of sparse crop.

Acknowledgements

The author would like to acknowledge the financial support of the UK Overseas Development Administration for this study which formed part of the Sparse Crop Evaporation Experiment. Also the author would like to thank the staff of the ICRISAT Sahelian Centre who have assisted in the establishment of Institute of Hydrology research in Niger.

References

Buettner, K.J.K. and Kern, K.D., 1965. The determination of infrared emissivities of terrestrial surfaces. *J. Geophys. Res.*, 70, 1329-1337.

Fuchs, M. and Tanner, C.B., 1966. Infrared thermometry of vegetation. *Agron. J.*, 58, 597-601.

Fuchs, M. and Tanner, C.B., 1967. Evaporation from a drying soil. *J. Appl. Meteor.*, 6, 852-857.

Fuchs, M. and Tanner, C.B., 1968. Surface temperature measurements of bare soils. *J. Appl. Meteor.*, 7, 303-305.

Huband, N.D.S., 1985. An infrared radiometer for measuring surface temperature in the field. Part 1. Design and construction. *Agric. For. Meteorol.*, 34, 215-226.

Idso, S.B., Jackson, R.D., Ehvier, W.L. and Mitchell, S.T., 1969. A method of determining the infrared emittance of leaves. *Ecology*, 50, 899-902.

Kalma, J.D., Aiksins, H. and Laughlin, G.P., 1988. Calibration of small infrared temperature transducers. *Agric. For. Meteorol.*, 43, 83-98.

Ross, J., 1981. The radiation regime and architecture of plant stands. *Tasks for vegetation sciences* 3: (Helmut Leith, Ed.) Dr. W. Junk Publishers. The Hague, 391 pp.

West, L.T., Wilding, L.P., Landeck, J.K. and Calhoun, F.G., 1984. Soil survey of the ICRISAT Sahelian Centre, Niger, West Africa. Soil and Crop Sciences Department/Topsoils, Texas A & M University System, College Station, Texas.

Wright, I.R., 1990. A laboratory calibration of infrared thermometers. *Int. J. Remote Sensing*, 11, 181-186.

Appendix 1

MIKRON PORTABLE INFRARED THERMOMETER CALIBRATION NOTES

An attempt was made to repeat the calibration of the Mikron portable infrared thermometer conducted by J.S. Wallace between September 1984 and March 1987 (personal communication). During these earlier calibrations the instrument was left switched on (idle but self-calibrating) and clamped to look down onto a volume of water at various known temperatures; the body of the instrument was at approximately room temperature, 25°C. Readings were noted by depressing the instrument trigger in situ. The resultant calibration yielded a series of straight-line regressions, with gradients close to unity, but with higher gradients (1.15) at lower temperatures (10°C) and lower gradients (0.92) at higher temperatures (60°C): this is shown in Figure A1.1.

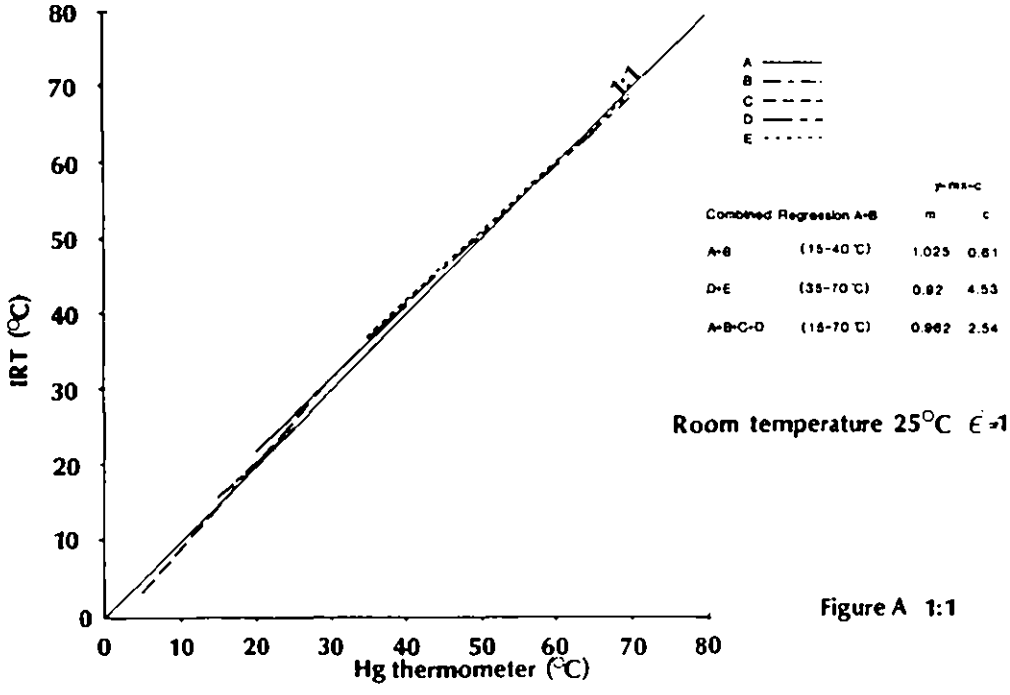

Figure A1.1 Mikron IRT calibrations over water.

The calibration discussed here was conducted using an environment chamber so that the instrument and/or the calibration surface (a solid plate of matt black aluminium) could be kept at a constant temperature.

No sensible result was obtained until the importance of the self-calibration (idle) status was acknowledged. The handbook states that "... (before pressing the trigger to take a reading) ... Aim the Mikron 80 at the floor or at an object near ambient (room) temperature; wait a few seconds".

When the instrument was allowed to self-calibrate at a constant temperature of

25°C (viewed surface and instrument body), a straight line calibration was obtained fom 8° to 75°C with a gradient of 0.8. Then with self-calibration at a temperature of 13°C a different straight line was obtained but with the same gradient (Figure A1.2).

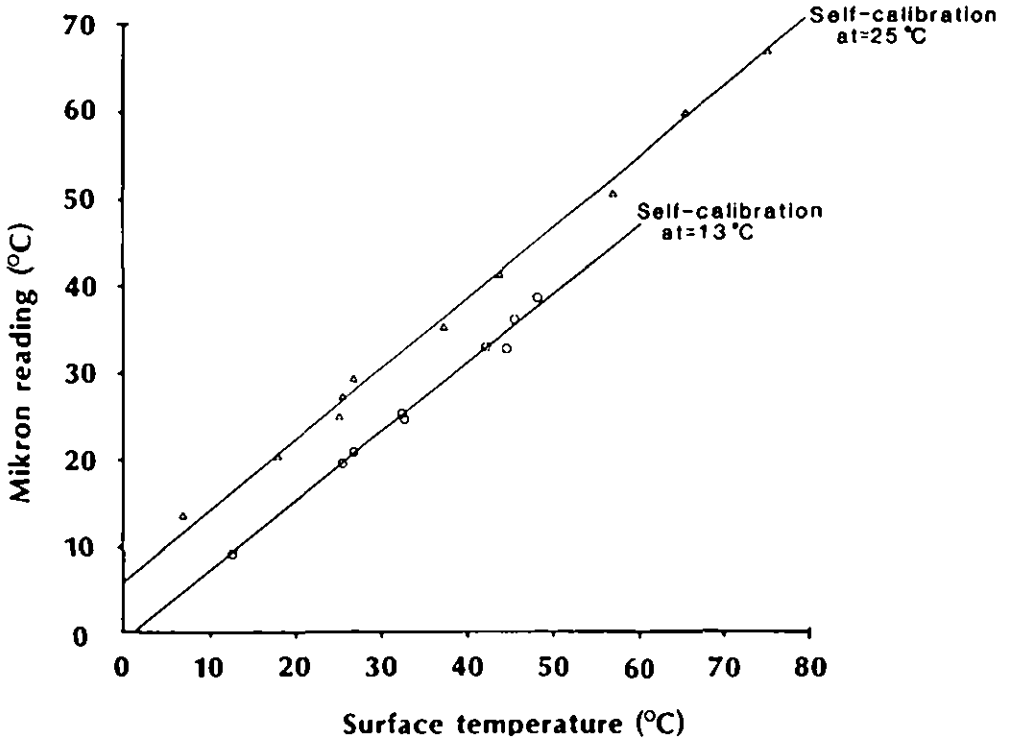

Figure A1.2 Mikron IRT calibrations at constant self-calibration temperature in an environment chamber.

Similarly, when the calibration surface was kept at a constant temperature of 25°C a linear relationship was indicated between the self-calibration temperature and the Mikron reading (Figure A1.3) indicating a simple multiple function.

When all of these calibration points are combined in a multiple regression the resultant equation is:

$$T_s = 1.23\ T_r - 0.606\ T_m + 8.53 \quad (r^2 = 0.98) \qquad \text{A.1}$$

where T_s is an estimate of the true surface temperature
T_r is the Mikron reading
and T_m is the self-calibration temperature:
which is the temperature of the instrument body AND the temperature of the surface being viewed by the instrument aperture.

It must be noted that time did not allow the temperature, T_m, to be split into two separate variables and increase the complexity of the calibration. Therefore, it is not possible to comment in detail on the calibrations conducted by Wallace; in his calibration the instrument body was near room

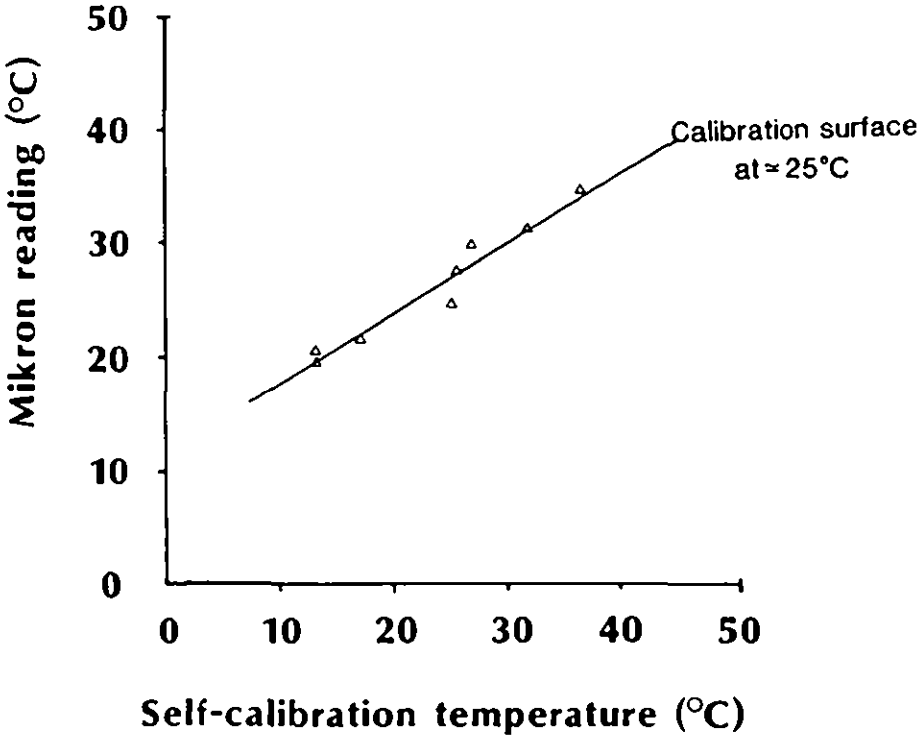

Figure A1.3 Mikron IRT calibration at constant surface temperature in an environment chamber.

temperature while the surface viewed during self-calibration was that of the water at temperatures ranging from 5° to 70°C.

Subsequent trials have shown that, whereas the temperature of the viewed surface cannot be neglected during self-calibration, the temperature of the instrument body is the more important influence on the Mikron reading. Furthermore, if it is assumed that in Wallace's calibration the body of the instrument, suspended above the hot (or cold) water, has its temperature raised (or lowered) by the proximity of the water, then the resultant synthesized calibration is similar to that of Wallace's earlier work.

In detail, if the instrument body temperature deviates from ambient by 0.3 of the temperature difference between the instrument and the surface, or

$$T_m = 25 + 0.3 \quad (T_s - 25) \qquad \text{A.2}$$

then, when substituted into Equation A.1, it is possible to synthesize a very similar calibration to that of Wallace, dependant on the value 0.3 which has been chosen to show a good fit (Figure A1.4). This suggests that the results of the two calibration methods are not necessarily inconsistent.

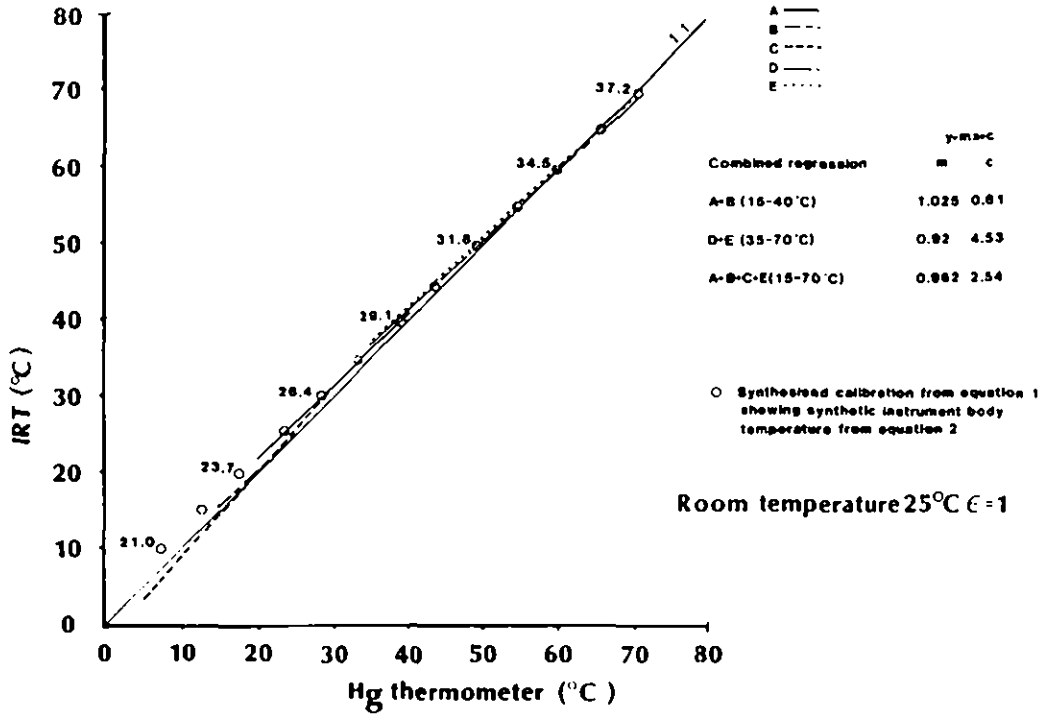

Figure A1.4 Mikron IRT calibration over water compared with modelled data.

RECOMMENDATION

The work described here represents the basis for a workable field technique. Better estimates of surface temperature can be made by monitoring the self-calibration temperature in hot (or cold) environments where it is not possible to maintain the instrument body at calibration temperature.

In the field, and until further work can indicate any improvement, the best estimate of surface temperature can be calculated from Equation A.1 if the instrument is kept in a shielded box with its internal temperature close to ambient and containing a mercury-in-glass thermometer so that the self-calibration temperature, T_m, can be recorded. Also the instrument should be shielded from direct sunlight when removed from the box for use.

Appendix 2

DERIVATION OF AN EXPRESSION FOR THE RADIATION RECEIVED AT A PLANAR SURFACE FROM AN ANNUAL PORTION OF A SURROUNDING HEMISPHERICAL UNIFORM EMITTER

Irradiance, dR, of unit area of horizontal surface from a small portion of surrounding hemispherical emitter, $rd\phi dc$, at zenith angle ϕ, is given by the radiance of the emitter, N, constrained by the solid angle, ω, subtended by the unit area:

$$dR = N.\ rd\phi dc.\omega \qquad (A2.1)$$

where $rd\phi$ is the thickness of the annulus and dc is a small increment of its circumference.

$$\text{As} \quad \omega = \text{unit area} \times \text{Cos}\phi/r^2 \qquad (A2.2)$$

$$\text{then} \quad dR = \frac{N}{r}\,\text{Cos}\phi\ d\phi dc \qquad (A2.3)$$

Expanding equation A2.3 to represent the circumference of the annulus by replacing dc with $C = 2\pi r\text{Sin}\phi$ gives:

$$dR = 2\pi N\ \text{Cos}\phi\ \text{Sin}\phi\ d\phi$$

$$\text{or} \quad R = 2\pi N \int_{\phi=0}^{\phi=\pi/2} \text{Cos}\phi\ \text{Sin}\phi\ d\phi \qquad (A2.4)$$